Journal of Neuroscience Methods 255 (2015) 104–114

Contents lists available at ScienceDirect

Journal of Neuroscience Methods

journal homepage: www.elsevier.com/locate/jneumeth

Computational Neuroscience

Automatic segmentation of the lateral geniculate nucleus: Application to control and glaucoma patients

Jieqiong Wang[a,b], Wen Miao[a,b], Jing Li[c], Meng Li[a,f], Zonglei Zhen[d], Bernhard Sabel[e], Junfang Xian[c], Huiguang He[a,b,*]

[a] State Key Laboratory of Management and Control for Complex Systems, Institute of Automation, Chinese Academy of Sciences, Beijing 10090, China
[b] Key Laboratory of Molecular Imaging of Chinese Academy of Sciences, Institute of Automation, Chinese Academy of Sciences, Beijing 10090, China
[c] Department of Radiology, Beijing Tongren Hospital, Capital Medical University, Beijing 100730, China
[d] National Key Laboratory of Cognitive Neuroscience and Learning, Beijing Normal University, Beijing 100875, China
[e] Otto-von-Guericke University of Magdeburg, Medical Faculty, Institute of Medical Psychology, Magdeburg, Germany
[f] Department of Neurology, Otto-von-Guericke University, Germany

HIGHLIGHTS

- We provide an automatic LGN segmentation method, which is objective, efficient, valid and applicable.
- We find the LGN asymmetry and LGN atrophy along with the human age.
- We find that the bilateral LGN volumes shrinks in glaucoma patients and the LGN volumes are correlated with clinical parameters in patients.

ARTICLE INFO

Article history:
Received 23 April 2015
Received in revised form 5 August 2015
Accepted 6 August 2015
Available online 14 August 2015

Keywords:
Automatic segmentation
LGN
Structural MRI
Vision

ABSTRACT

Background: The lateral geniculate nucleus (LGN) is a key relay center of the visual system. Because the LGN morphology is affected by different diseases, it is of interest to analyze its morphology by segmentation. However, existing LGN segmentation methods are non-automatic, inefficient and prone to experimenters' bias.
New method: To address these problems, we proposed an automatic LGN segmentation algorithm based on T1-weighted imaging. First, the prior information of LGN was used to create a prior mask. Then region growing was applied to delineate LGN. We evaluated this automatic LGN segmentation method by (1) comparison with manually segmented LGN, (2) anatomically locating LGN in the visual system via LGN-based tractography, (3) application to control and glaucoma patients.
Results: The similarity coefficients of automatic segmented LGN and manually segmented one are 0.72 (0.06) for the left LGN and 0.77 (0.07) for the right LGN. LGN-based tractography shows the subcortical pathway seeding from LGN passes the optic tract and also reaches V1 through the optic radiation, which is consistent with the LGN location in the visual system. In addition, LGN asymmetry as well as LGN atrophy along with age is observed in normal controls. The investigation of glaucoma effects on LGN volumes demonstrates that the bilateral LGN volumes shrink in patients.
Comparison with existing methods: The automatic LGN segmentation is objective, efficient, valid and applicable.
Conclusions: Experiment results proved the validity and applicability of the algorithm. Our method will speed up the research on visual system and greatly enhance studies of different vision-related diseases.

1. Introduction

The lateral geniculate nucleus (LGN) is the primary visual relay center of the brain that receives retinofugal fibers and transmits visual information to the visual cortex (Sherman and Koch, 1986). The structure and function of the LGN (Schneider et al., 2004; Zhang et al., 2010; McKetton and Schneider, 2012; McKetton et al., 2013) and its relationship with other structures of the visual

* Corresponding author at: ZhongGuanCun East Rd. 95#, Beijing 100190, China. Tel.: +86 10 82544621; fax: +86 10 82544621.
E-mail addresses: jieqiong.wang@ia.ac.cn (J. Wang), mwinvent@gmail.com (W. Miao), lijingxbhtr@163.Com (J. Li), albertleemon@gmail.com (M. Li), zhenzonglei@Qq.Com (Z. Zhen), bernhard.Sabel@Med.Ovgu.De (B. Sabel), cjr.Xianjunfang@Vip.163.Com (J. Xian), huiguang.he@ia.ac.cn (H. He).

http://dx.doi.org/10.1016/j.jneumeth.2015.08.006
0165-0270/

pathway (such as optic tract and primary visual cortex (Kupfer et al., 1967; Andrews et al., 1997)) have been extensively studied. The LGN is affected by ophthalmological diseases such as myopia (von Noorden et al., 1983; von Noorden and Crawford, 1992; Miki et al., 2003; Barnes et al., 2010) and glaucoma (Gupta et al., 2009; Weber et al., 2000; Dai et al., 2011; Chen et al., 2013) and hence of clinical interest. But all these quantitative MRI studies are based on manual or semi-automatic segmentation methods that are prone to human error of judgment. This limits existing analysis methods in their objectivity, efficiency, validity and applicability of LGN measurements, making conclusions based on them less deterministic.

Except for aforementioned manual or semi-automatic LGN segmentation methods, another method is to apply LGN atlas to guide LGN segmentation by registering it to the individual space. Only two LGN atlases exist to date: the Talairach atlas (Lancaster et al., 2000) and the WFU PickAtlas (Maldjian et al., 2003). However, both were built based on postmortem sections of a single case of a 60-year-old French female. The brain size in these sections was smaller than the average brain sizes because the brain of the subject was atrophied because of old age and death. Thus, the segmented LGN using these prior atlases as a reference point underestimates the true LGN volume compared to those reported in previous studies (Andrews et al., 1997; Putnam, 1926; Zvorykin, 1980), seriously limiting the validity of LGN morphology. In addition, using a single case as a reference point does not consider that LGN volumes vary between subjects and vary along with human age (Li et al., 2012). Thus, prior atlases cannot be used to objectively, reliably and validly determine the normative LGN volume, which is needed as a reference for any MRI studies of the LGN such as to study the influence of age, hemispheric asymmetry, sex, disease, etc. We believe that only a fully automatic LGN segmentation method could overcome the limitations in previous studies.

In this paper, we proposed an automatic LGN segmentation method based on structural MRI imaging. The validity of segmentation method was proved by comparing with the manually segmented LGN as well as LGN location in visual system. The applicability of the method was demonstrated by investigating the property of LGN volumes in normal controls and glaucoma effects on LGN volumes.

2. Materials and methods

2.1. Subjects & MRI image acquisition

2.1.1. Dataset 1

We chose healthy subjects from the publicly available Information extraction from Images (IXI) database (http://www.brain-development.org/) and applied their T1-weighted images and DTI images in this study. The IXI database contained T1-weighted images from 580 normal subjects and DTI images from only 397 normal subjects from Hammersmith Hospital and Guy's Hospital (scanning parameters can be found on the official website: http://www.brain-development.org/). We excluded several subjects if one of the following criteria applied: (i) subjects without T1-weighted images or DTI images; (ii) no age or sex information was available; and (iii) the images failed to be properly recognized during the image processing. Finally, 280 normal subjects aged 20–84 years (age ± SD = 51.32 ± 15.38, male/female: 115/165, age distribution: Fig. S1) were taken from the IXI database and further analyzed.

2.1.2. Dataset 2

All the subjects in Dataset 2 were recruited by Beijing Tongren Hospital. The Medical Ethics Committee of the Beijing Tongren Hospital approved this study and all participants have signed the informed consent form after explained the nature and design of the study. Dataset 2 included 25 primary open angle glaucoma (POAG) patients (age: 44.6 ± 13.0 years, male/female: 11/14) and 25 age-sex-matched normal controls (age: 36.8 ± 11.6 years, male/female: 13/12). All participants were right-handed Chinese. The normal controls were checked to assure that (1) they had no eye diseases or glaucoma; (2) they had no psychiatric disorders; (3) they had no smoking or drinking in the past three months. The subjects in glaucoma group were diagnosed as POAG by experts in Beijing Tongren Hospital. All patients (1) had no other eye diseases; (2) had no psychiatric disorders; (3) no smoking or drinking in the past 3 months.

The patients voluntarily chose to take further examinations including retinal nerve fiber layer (RNFL), cup-to-disk ratio (CDR) and visual field (VF). The demographic data of patients is shown in Table 1. Complete clinical parameters of 14 patients were collected.

Table 1
Demographic data of primary open angle glaucoma patients. "√" represents the information is available, "–" represents the information is not available.

No.	Sex	Age	RNFL		CDR		VF	
			Left	Right	Left	Right	Left	Right
1	F	17	√	√	√	√	√	√
2	F	47	√	√	√	√	√	√
3	M	56	–	–	–	–	√	√
4	M	59	√	√	√	√	√	√
5	M	52	√	√	√	√	√	√
6	M	60	√	√	√	√	√	√
7	F	56	–	–	√	√	√	√
8	F	23	–	–	–	–	–	–
9	M	68	√	√	√	√	√	√
10	M	18	√	√	√	√	√	√
11	F	46	–	–	–	–	–	–
12	M	28	–	–	–	–	√	√
13	F	48	√	√	√	√	√	√
14	F	58	√	–	√	√	√	–
15	M	29	√	√	√	√	√	√
16	F	47	–	–	–	–	–	–
17	F	40	√	√	√	√	√	√
18	M	55	√	√	√	√	√	√
19	F	22	–	–	√	√	√	√
20	F	21	–	–	–	–	–	–
21	M	75	√	√	√	√	√	√
22	F	41	√	√	√	√	√	√
23	M	59	√	√	√	√	–	–
24	F	47	–	–	–	–	√	√
25	F	44	√	√	√	√	√	√

All participants were scanned in a GE 3 T scanner to acquire T1-weighted structural MRI images with the following scanner parameters: TR/TE = 8.9/3.5 ms, slice thickness = 1 mm, flip angle = 13°, matrix = 256 × 256, FOV = 24 × 24 cm^2, slice number = 209, and slice resolution = 0.9999 × 0.9375 mm^2.

2.2. Automatic LGN segmentation

The pipeline of automatic LGN segmentation is shown in Fig. 1. The main procedure includes image preprocessing, prior mask production and LGN delineation by region growing. The steps were as follows:

2.2.1. Image preprocessing

For image preprocessing, all subjects' T1-weighted images were firstly performed correction of non-uniform intensity by using the N3 algorithm (Sled et al., 1998). Then skull stripping was done for the whole brain, which was subsequently segmented to label neuroanatomical structures in the human brain using a method described in (Fischl et al., 2002), which is performed by the software FreeSurfer (Version 5.0.0, https://surfer.nmr.mgh.harvard.edu). Thereafter, the ventral diencephalon area (VDC) was chosen

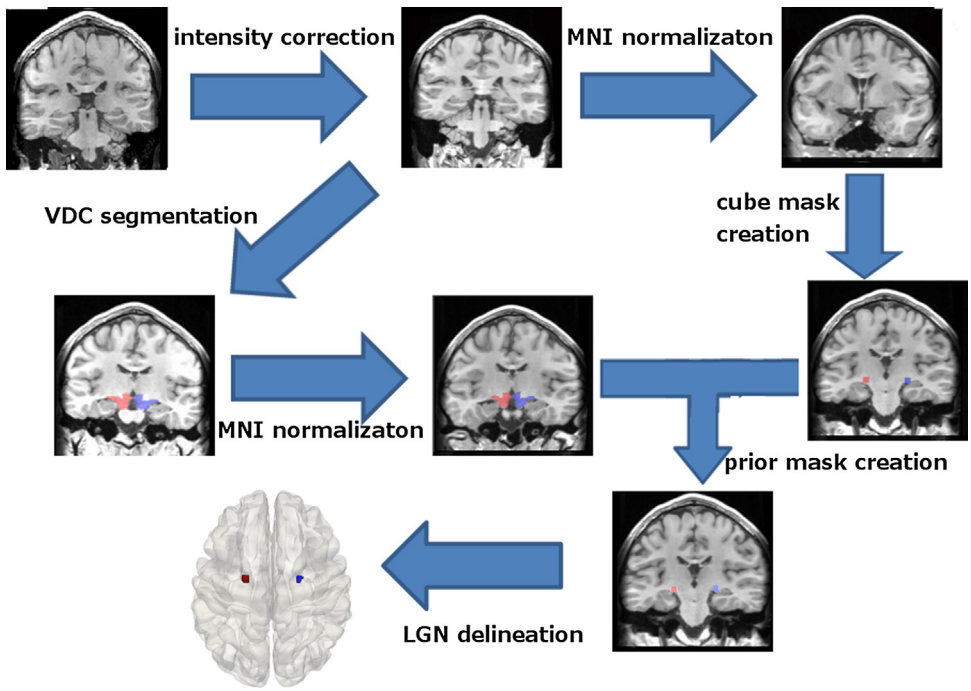

Fig. 1. Pipeline flow chart of automatic LGN segmentation.

from automatic subcortical segmentation to generate a VDC mask since the majority of the posterior tissue of VDC is LGN (Desikan et al., 2006).

In order to apply the prior information and construct the atlas in MNI space, the corrected images and VDC masks were then normalized to MNI space by the software SPM8 (http://www.fil.ion.ucl.ac.uk/spm/) Firstly, we performed a 12-parameter affine transformation (Ashburner et al., 1997) to match the corrected images. Then a nonlinear registration (Ashburner et al., 1998) was applied to minimize the difference between the corrected images and the MNI template. The spatially normalized images were resampled to 1 mm × 1 mm × 1 mm in a matrix dimension of 181/217/181. After normalizing corrected images to the MNI space, we used the parameters obtained in the corrected images normalization to register VDC masks to MNI space.

2.2.2. Prior mask generation in MNI space

Kastner's work (Kastner et al., 2004) demonstrated that estimates of mean human LGN location were [−23.33, −21, −4.66] and [22.88, −21.3, −4.63] in stereotaxic space for the left and right LGN, respectively. After coordinate conversion to MNI space, the center of the left human LGN was located at P_l [−23, −22, −7] and that of the right human LGN at P_r [26, −22, −8]. Moreover, previous anatomical studies (Andrews et al., 1997; Chen et al., 1998) showed that LGN approximated as a cube with a side length of 5 mm. Based on this prior information, we respectively built a cube mask centered as P_l or P_r with a side length of 7 mm (considering the error caused by normalization) for the left and right LGN in the MNI space. Then the VDC mask and the cube mask were intersected to obtain the LGN prior mask. The region limited by this prior mask was defined as prior-mask-restricted region. We subsequently tried to isolate LGN in this prior-mask-restricted region.

2.2.3. LGN delineation

Seeded region growing was used to isolate LGN in the prior-mask-restricted region. This seeded region growing was proposed before (Adams and Bischof, 1994) which permits the examination of neighboring voxels of the starting point and determine whether the voxel neighbors should be added to the segmentation results. We noted the ith voxel in the prior-mask-restricted region as $P_i (i = 1, 2, \ldots, N)$, the coordinate of P_i as V_i, the intensity of P_i as I_i. The gravity center of bilateral LGN P_l/P_r was chosen as the started point P_s, respectively. The LGN region was defined as:

$$LGN = \bigcup_{i=1}^{N} P_i, \quad (i = 1, 2, \ldots, N) \quad \text{if} \quad ||V_i - V_s|| \le R_0, \quad I_i - I_s| \le I_0 \tag{1}$$

where we chose 30 for the threshold of gray value I_0 and 5 mm for R_0 (noted as RG5), respectively. The value of I_0 was determined by experience. The radius R_0 was determined by the experiments, which will be introduced in the following part. Then we could delineate LGN according to Eq. (1).

Selection of radius in region growing

For all T1-weighted images of 280 subjects in Dataset 1, we performed the automatic LGN segmentation by region growing with different radii (3 mm/4 mm/5 mm), respectively. We did not conduct region growing with radius over 5 mm, since the sphere with radius 5 mm centered at the mean LGN center almost cover all prior-mask-restricted region. The STAPLE algorithm is a straightforward method to compare the different segmentation results, because it constructs an estimated reference standard based on all the segmentations and assesses the segmentation methods by the similar measures with the standard (Warfield et al., 2004). It was revealed that Williams' index (Williams, 1976) gave the similar results to STAPLE. The larger Williams' index is, the better the segmentation is. Considering the fast and easy computation of Williams' index, we compared the LGN segmentation results of region growing with three radii by Williams' index (Williams, 1976) to select the appropriate radius of region growing.

We note $X_j (j = 1, 2, 3)$ as the set of voxels label 1 or 0 in the prior-mask-restricted region by region growing with different radius. Williams' index for region growing with different radius is defined as

$$WI_j = \frac{\sum_{j' \neq j}^{3} JC(X_j, X_{j'})}{2\sum_{j' \neq j}^{3} \sum_{j'' \neq j}^{j'-1} JC(X_{j'}, X_{j''})}, \tag{2}$$

where $JC(X_j, X_{j'}) = \left|X_j \cap X_{j'}\right| / \left|X_j \cup X_{j'}\right|$ is the similarity measure between two different segmented LGN results. If Williams' index is over one, the method *j* agrees with the other methods at least as well as they agree with each other.

2.3. Evaluation

We chose 24 subjects[1] from 280 subjects in Dataset 1, and then three experts manually segment LGN of these 24 subjects. The average result of the manually segmented LGNs was treated as the reference LGN. Then we calculated the Dice coefficient (DC) (Hripcsak and Heitjan, 2002) Eq. (3) and used DC as the similarity measure between the automatic segmented LGN and the reference LGN:

$$\mathrm{DC} = \frac{2\left|A \cap B\right|}{\left|A\right| + \left|B\right|}, \tag{3}$$

where *A* and *B* represent the automatic segmented LGN and the reference LGN, respectively. If there is no overlap between *A* and *B*, DC is 0. If *A* and *B* are exactly overlapped, DC is 1.

However, the manual LGN segmentation is not objective because of the subjective judgments of the expert. Even though we took the average manual LGN as the reference LGN to reduce the bias caused by experts' subjectiveness, the reference LGN was still not the accurate ground-truth LGN. Therefore, we also evaluated the automatic LGN segmentation indirectly from three perspectives: (1) the anatomical location of LGN; (2) LGN volumes in normal controls; (3) glaucoma effects on LGN volumes.

2.3.1. The anatomical location of LGN

Since LGN is the conjunction of optic tract and optic radiation as well as all the thalamocortical fibers from the LGN project to the primary visual cortex (V1) through the optic radiation, we further validated our segmented LGN by tracking white matter from LGN to V1 with DTI imaging.

All DTI images of 280 subjects in Dataset 1 were analyzed by the FMRIB's Diffusion Toolbox (FDT) (Behrens et al., 2003). In short, eddy current correction was firstly performed to correct stretches and shears in the DTI images. Then the whole brain was skull stripped and distributions on diffusion parameters at each voxel were built up for probabilistic tractography and the segmented LGN was registered to the least diffusion-weighted image (b0) space. Next, the registered LGN was chosen as the seed mask for the probabilistic tractography.

We also compared the probability of tracking from the segmented LGN to V1 with that of tracking from 100 random templates to V1. The 100 cube templates had the same volume as the mean segmented LGN volume in the brain area except V1. Then a two-sample *t*-test was applied to assess the difference between the probability of tracking from the segmented LGN to V1 and that of tracking from random templates to V1.

2.3.2. LGN volumes in normal controls

We transformed inversely our segmented LGN of 280 subjects in Dataset 1 in MNI space to the native space and compared our automatic segmented results with previous studies (Putnam, 1926; Zvorykin, 1980; Li et al., 2012) to evaluate our segmented LGN volume range.

Moreover, we investigated the LGN asymmetry by conducting the paired *t*-test to compare the LGN volume between both hemispheres, and the gender effects on LGN volumes by conducting a two-sample *t*-test to compare the LGN volume difference between the male and the female. Finally, we performed correlation analysis to investigate age effects on the LGN volume.

When comparing the LGN volume difference between the male and female by the two-sample *t* test, we chose 104 males (49.85 ± 14.62 years) and 114 age-matched females (51.94 ± 14.53 years) from 280 subjects in Dataset 1. We further normalized LGN volume by intracranial volume (ICV) to regress out the influence of ICV.

The LGN in each hemisphere receives the information obtained by bilateral eyes at the same time, we hence investigated the relationship between mean volume of bilateral LGN and age. Considering the effects of ICV and sex, we calculated the Pearson coefficient between the mean LGN volume and age with ICV and sex as control variables.

2.3.3. Glaucoma effects on LGN volumes

In order to validate the applicability of automatic LGN segmentation, we investigated the alterations of LGN volumes in glaucoma patients. We applied the LGN segmentation algorithm to segment LGNs of normal controls and glaucoma patients in Dataset 2. Then we conducted a two-sample *t*-test to compare the LGN volumes between normal controls and glaucoma patients with ICV as control variable. In addition, we calculated the partial correlation coefficients between the LGN volume and CDR as well as that between the LGN volume and VF (taking age, gender and ICV as control variables) in glaucoma patients to further investigate the relationship between the LGN volume and clinical parameters.

3. Results

3.1. Selection of radius in region growing

Fig. 2 shows the Williams' index of segmented LGN obtained by region growing with different radius (3 mm/4 mm/5 mm). The red represents the results of left LGN and the blue represents the results of right LGN. From this Fig., we can see that region growing with radius 5 mm outperformed region growing with the other radii. Therefore, the most appropriate radius of region growing for LGN segmentation is 5 mm.

3.2. Comparison with manually segmented LGN

After comparing with the manually segmented LGN, we found that the DCs of bilateral automatic segmented LGN were 0.72 (0.06) for the left LGN and 0.77 (0.07) for the right LGN.

3.3. The anatomical location of LGN

In order to evaluate the anatomical location of segmented LGN, we performed probabilistic tractography seeding from segmented LGN. Fig. 3 shows the resulting representative anatomical path seeding from LGN. Here, the subcortical pathway passes the optic tract (top row) and reaches V1 through the optic radiation (bottom row). This is consistent with the known anatomy that LGN is the primary visual relay center of the visual system (Sherman and Koch, 1986).

After comparing the probability of tracking from the segmented LGN to V1 with that of tracking from 100 random non-LGN templates to V1, we find that the probability of tracking from the segmented LGN to V1 is significantly higher than that of tracking from random templates to V1 ($p < 0.05$). This result demonstrates that the segmented LGN by RG5 is reliable in terms of anatomical location and its connection. Fig. 4 shows the 3D visualization of tracking results from seeding the bilateral LGN and two random non-LGN templates of one subject. V1 is labeled as green. The tracking results from the left LGN and the right LGN are labeled as red and

[1] Details of the selection procedures can be found in supplementary materials.

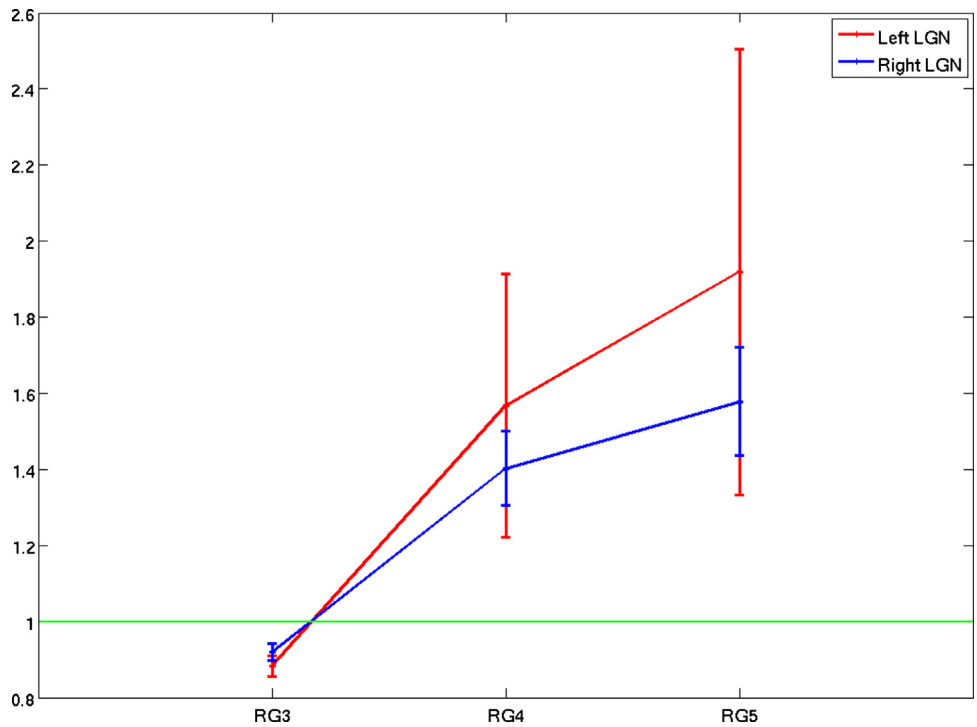

Fig. 2. Williams' index of segmented LGN obtained by region growing with different radii. RGr represents region growing with radius *r* mm. The red represents the results of left LGN and the blue represents the results of right LGN. (For interpretation of the references to color in this figure legend, the reader is referred to the web version of this article.)

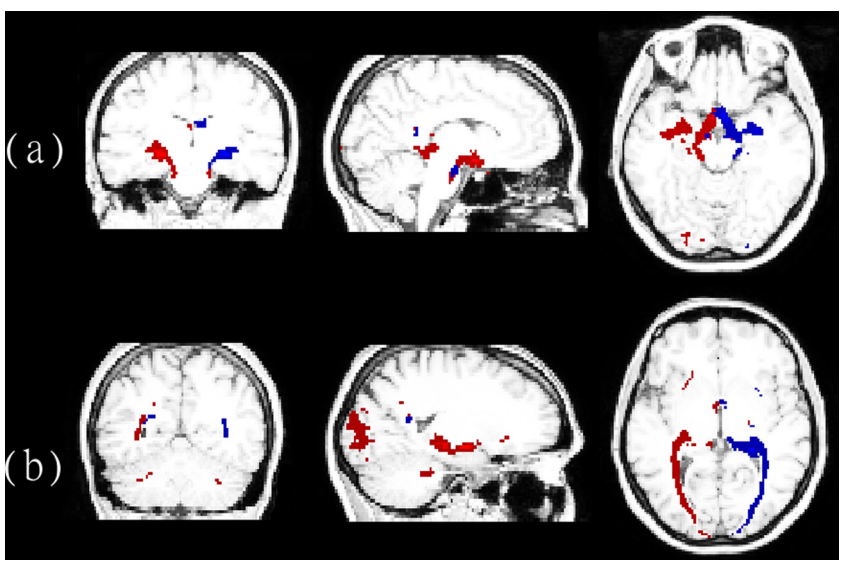

Fig. 3. Example of coronal, sagittal, and horizontal (left to right) of MRI images showing representative anatomical path seeding from LGN via probabilistic tractography. Red stands for the track result of the left LGN and blue of the right LGN. The upper row (a) shows the subcortical pathway passing through the optic tract and the lower row (b) shows the subcortical pathway reaching V1 through the optic radiation. (For interpretation of the references to color in this figure legend, the reader is referred to the web version of this article.)

blue, respectively. The tracking results from two random templates, one in the left and the other in the right hemisphere, are labeled in yellow and purple. From Fig. 4, we can also clearly see that there are much more tracking results to V1 (green) from the LGN (red and blue) than from random templates (brown and purple).

3.4. LGN volumes in normal controls

Table 2 shows the LGN volume range obtained in different studies. The first column is the result of our segmented LGN. Column 2 to Column 4 shows the results of previous postmortem studies. The last column shows the result of semi-automatic segmented LGN. In the postmortem studies, Putnam (Putnam, 1926) reported that the LGN volume range was 77–115 mm^3, Zvorykin (Zvorykin, 1980) reported that the LGN volume range was 66–152 mm^3, while Andrew (Andrews et al., 1997) reported the LGN volume range was 91–157 mm^3. The volume range of LGN obtained by semi-automatic segmentation (Li et al., 2012) is 52–105 mm^3 while that of our segmented LGN is 70–170 mm^3. It shows that our LGN volume range is slightly wider than that in previous studies.

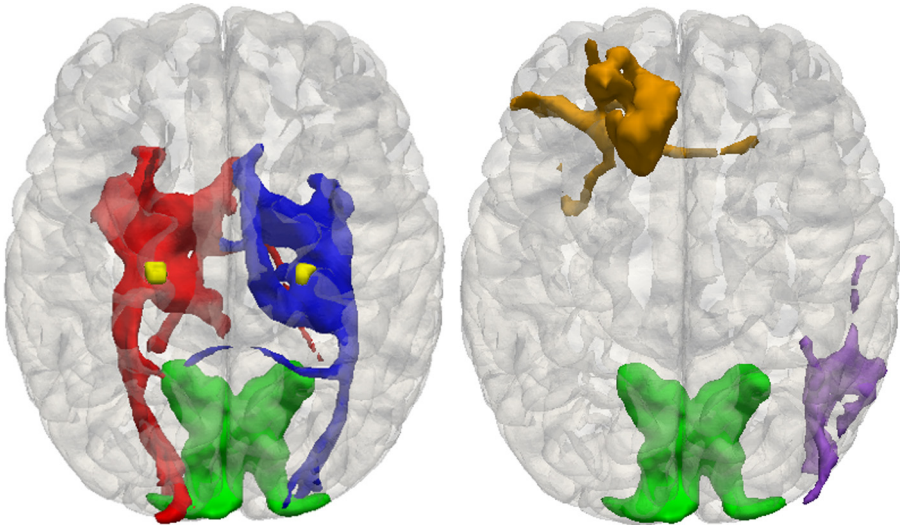

Fig. 4. Tracking results from different seed masks of one representative subject shown on b0 image. The left panel shows the results of our automatic segmentation method to identify the location of the LGN and visual cortex (V1) in the brain, where yellow represents the location of LGN, green represents the location of V1, red the tracking result from seeding the left LGN, blue shows the tracking results from seeding the right LGN. The right panel displays tracking result from seeding two random templates in the brain (purple and brown). (For interpretation of the references to color in this figure legend, the reader is referred to the web version of this article.)

Table 2
Comparison of LGN volumes obtained in different studies. N.A. = not available.

	RG5	Putnam (1926)	Zvorykin (1980)	Andrews et al. (1997)	Li et al. (2012)
Subjects num.	280	3	17	15	55
Age range	20–84	N.A.	N.A.	28–86	20–67
Volume range (mm^3)	70–170	77–115	66–152	91–157	52–105

Table 3
LGN volume differences between the male and the female by two-sample *t*-test. M, male; F, female.

	Hemisphere	M (mm^3)	F (mm^3)	M–F (mm^3)	*p*-Value
Native LGN volume	Left	136.63 (32.74)	122.11 (29.33)	14.52 (3.96)	<0.001
	Right	120.69 (29.22)	105.47 (22.78)	15.22 (3.30)	<0.001
	Mean	128.66 (25.00)	113.79 (19.37)	14.87 (2.82)	<0.001
Normalized LGN volume	Left	125.28 (26.72)	131.43 (31.53)	−6.15 (3.81)	0.108
	Right	111.15 (27.24)	114.01 (25.61)	−2.87 (3.39)	0.398
	Mean	118.21 (20.50)	122.73 (21.40)	−4.51 (2.71)	0.097

The automatic LGN segmentation was applied to investigate the asymmetry of bilateral LGN, the LGN volume difference between the male and the female, as well as the relationship between the LGN volume and age of the subjects.

We conducted the paired *t*-test to compare the LGN volume between both hemispheres in normal controls. The average left LGN volume ($127.65 \pm 31.95\ mm^3$) was significantly larger (difference = 15.78 mm^3, $t = 7.40$, $p < 0.001$) than the average right LGN volume ($111.87 \pm 26.10\ mm^3$) (Fig. 5) and the LGN volumes on both sides were correlated ($r = 0.256$, $p < 0.001$).

Sex effects on the LGN volume are shown in Table 3 and Fig. 6. We can see that though native LGN volume differences between the male and the female is investigated (left/right/mean: $p < 0.001$), there is no sex difference in normalized LGN volume (left: $p = 0.108$, right: $p = 0.398$, mean: $p = 0.107$). This demonstrates that sex has no effect on the LGN volume.

We investigated the relationship between the mean LGN volume and age by linear regression with the brain size ICV and sex as the control variables. Fig. 7 shows the regression result. Here, we can see that the mean LGN volume is significantly negatively correlated with human age ($r = -0.209$, $p = 0.001$), which means that the LGN volume decreases along with human age. This result that a large age range is associated with a large LGN volume range is consistent with the prior observation (Li et al., 2012).

Table 4
Comparison LGN volumes between normal controls and glaucoma patients. NC, normal controls; PAT, glaucoma patients.

Hemisphere	NC (mm^3)	PAT (mm^3)	*p*-Value
Left	144.08 (32.63)	124.00 (28.48)	**0.025**
Right	116.80 (29.83)	90.84 (37.47)	**0.009**
Mean	130.44 (26.85)	107.42 (25.84)	**0.003**

Bold values indicate $p < 0.05$.

3.5. Glaucoma effects on LGN volumes

In order to further validate the applicability of our automatic LGN segmentation algorithm, we applied the algorithm to segment LGN in both normal controls and glaucoma patients and then compared the LGN volumes between two groups (Table 4 and Fig. 8). Compared to normal controls, glaucoma patients have significant volume shrinkages in the left/right LGN the left/right LGN (left: $p = 0.023$, right: $p = 0.007$) and the mean bilateral LGN volume ($p = 0.002$). In addition, we investigated the relationship between LGN volume and CDR/VF in glaucoma patients. The result (Fig. 9) shows that the left LGN volume was negatively correlated with bilateral CDR (left: $r = -0.643$, $p = 0.033$, right: $r = -0.610$, $p = 0.046$)

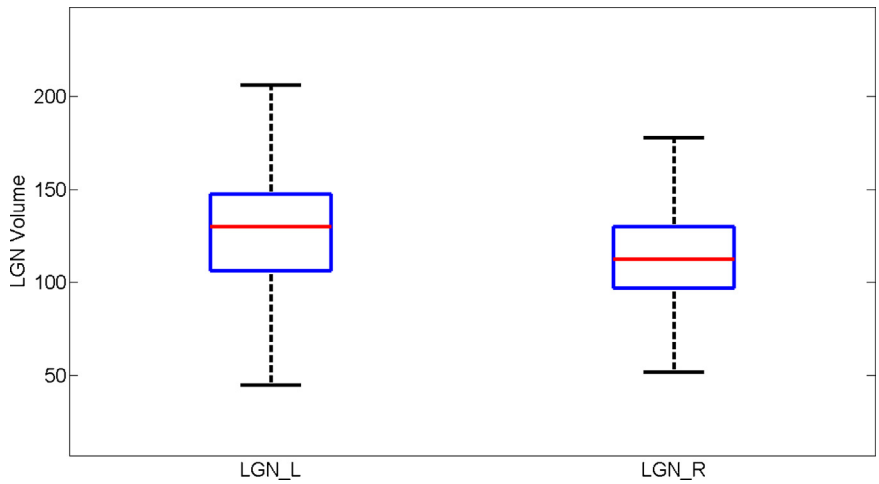

Fig. 5. Comparison of bilateral LGN volumes (mm^3). LGN_L: left LGN, LGN_R: right LGN.

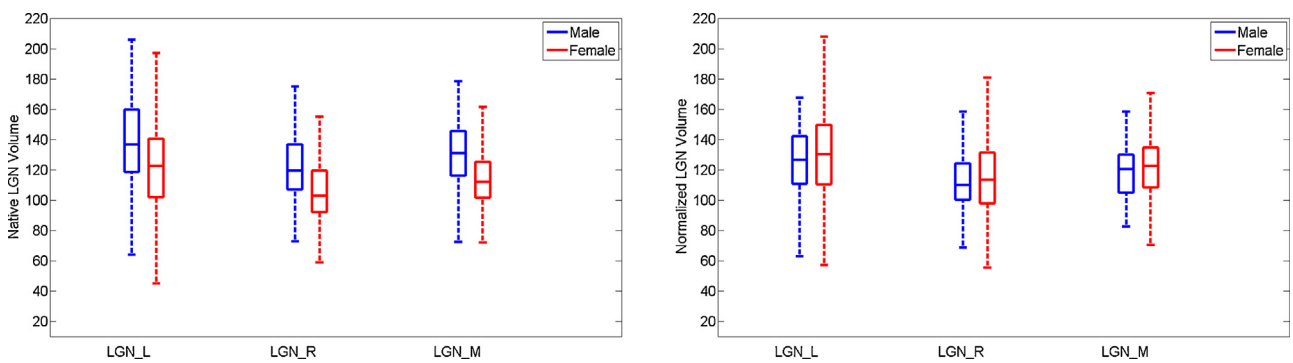

Fig. 6. Comparison of LGN volumes (mm^3) between male and female. The left panel shows the native LGN volume. The right panel shows the normalized LGN volume. LGN_L: left LGN, LGN_R: right LGN, LGN_M: the mean volume of bilateral LGN. Blue represents the LGN volume of the male. Red represents the LGN volume of the female. (For interpretation of the references to color in this figure legend, the reader is referred to the web version of this article.)

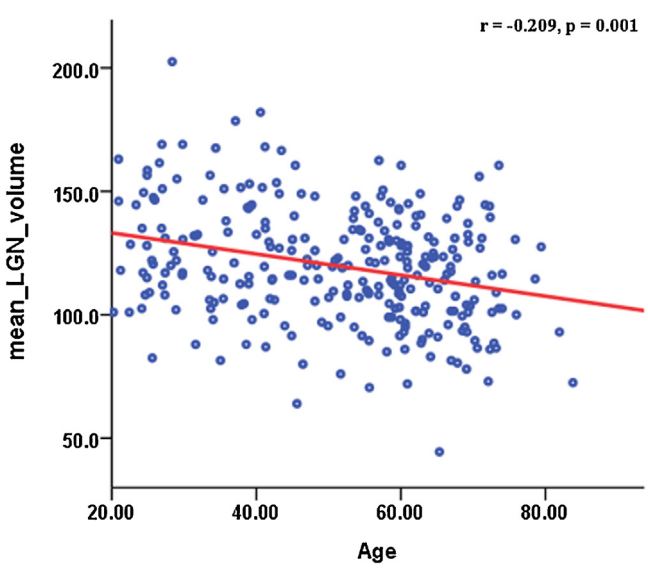

Fig. 7. The relationship between the mean LGN volume and human age with the brain size ICV and sex as the control variables.

(top row of Fig. 9). The right LGN volume was positively correlated with right VF size, i.e. small right LGN volume was associated with smaller visual field size ($r = 0.699$, $p = 0.017$) (left bottom of Fig. 9), and there was a tendency of a positive correlation with the left VF as well ($r = 0.534$, $p = 0.091$) (right bottom of Fig. 9).

4. Discussion

We presented an automatic segmentation method to locate and quantify the human LGN, using the method of region growing with a radius of 5 mm within the prior-mask-region. Then we evaluated the anatomical location of LGN, the LGN volumes in normal controls and glaucoma effects on LGN to prove the objectivity, efficiency, validity and applicability of the segmentation method, which are elaborated below.

4.1. Objectivity and efficiency

There are two ways to segment LGN: segmentation based on brain autopsy (Kupfer et al., 1967; Andrews et al., 1997; Putnam, 1926; Zvorykin, 1980; Decourten and Garey, 1982) and LGN segmentation in vivo. The former is exceedingly time-consuming and cannot be generalized to the living population at large. The latter includes manual LGN segmentation on PDWI (McKetton and Schneider, 2012; McKetton et al., 2013; Gupta et al., 2009; Horton et al., 1990; Fujita et al., 2001; Devlin et al., 2006; Giraldo et al., 2012; Viviano et al., 2012; Chica and Schneider, 2013), LGN detection on task-related fMRI with visual stimulus (Miki et al., 2003; Kastner et al., 2004; Chen et al., Jan 1998; Chen et al., 1999), manual LGN segmentation (Korsholm et al., 2007) or semi-automatic LGN segmentation (Li et al., 2012) on T1-weighted images. All manual segmentations are inefficient and not objective. For segmentation on PDWI, the rich structures in thalamic nuclei have various relaxation times and similar proton densities, which

precludes sufficient contrast to differentiate thalamic nuclei from each other (Kanowski et al., 2010). For LGN detection with fMRI, the activation area of LGN can be influenced by different factors, such as (i) age or impaired vision (D'Esposito et al., 2003; Behzadi and Liu, 2005; Lu et al., 2008), (ii) the different global normalization procedures (Miki et al., 2004), and (iii) activations from adjacent structures such as the pulvinar (Kastner et al., 2004; Chen et al., 1998). There is thus still controversy over the LGN detection with fMRI. For the semi-automatic method of T1-weighted imaging, the initial seed was determined by experts (Li et al., 2012). After image preprocessing, it still takes 8–10 min to segment the LGN for one subject. In short, all the current LGN segmentations are inefficient, imprecise and not objective. In contrast, our automatic LGN segmentation is superior in terms of both objectivity and efficiency. After image preprocessing, our method takes about 0.5 min per case whereas a manual segmentation takes 15 min and semi-automatic segmentation 8–10 min, which means that our methods is 16–30 times faster than other methods.

4.2. Validity

To our best knowledge, we are the first to use similarity coefficient to compare the segmented LGN with the manually segmented LGN directly. Noticing the challenge that the manually segmented LGN may not be accurately equivalent to the ground-truth LGN due to its small-scale structure, the similarity coefficients (left LGN: 0.72 ± 0.06, right LGN: 0.77 ± 0.07) are relatively high and well accepted.

We also validated the anatomical location of LGN indirectly by LGN-based tractography. The results of probabilistic tractography seeding from the segmented LGN (Fig. 3) show that the anatomical path seeding from our segmented LGN passes the optic tract and passes through the optic radiation toward V1. This connection of LGN to optic tract and V1 (through optic radiation) is a validation of the correct anatomical localization of LGN (Sherman and Koch, 1986; Ciccarelli et al., 2003).

4.3. Applicability

In order to evaluate the applicability of our LGN segmentation method, we investigated the LGN volumes in normal controls including the LGN volume range of normal control, LGN asymmetry and sex/age effects on LGN volumes, as well as glaucoma effects on LGN volumes.

4.3.1. LGN volumes in normal controls

In the three previous postmortem studies, the ranges of LGN volumes were 77–115 mm^3 (Putnam, 1926), 66–152 mm^3 (Zvorykin, 1980), and 91–157 mm^3 (Andrews et al., 1997), respectively. The semi-automatic LGN segmentation study (Li et al., 2012) reported LGN volume range as 52–105 mm^3. Our LGN volume range was 70–170 mm^3, which is a little wider than previous studies (Table 2). This is because the structures in the brain shrink with death and our LGN study includes a large sample of 280 health controls with a quite large age range (from 20 to 85 years). The study (Andrews et al., 1997) pointed out that the LGN volumes among individuals might vary as significantly as two or three times. The study (Li et al., 2012) indicated that mean bilateral LGN volume shrink along with human age (which was also demonstrated in the current study, shown in Fig. 7). Hence, the larger sample size and larger age range in our study lead to the greater variability than previous studies.

Both semi-automatic LGN segmentation study (Li et al., 2012) and the present results found asymmetry of LGN volumes between both hemispheres. However, the study (Li et al., 2012) demonstrated the right LGN volume is larger than the left LGN, which is contrary to our present result. The number of subjects in our work is 280, which is much larger than that in the study (Li et al., 2012) (only 55 subjects). This suggests that our result of LGN asymmetry may be more reliable than the study (Li et al., 2012). Currently, there are two atlases including LGN, which is the Talairach atlas (Lancaster et al., 2000) and the WFU atlas (Maldjian et al., 2003). Although the volumes of the bilateral LGN from the Talairach atlas are almost equal, the WFU atlas is more reliable than Talairach atlas (Maldjian et al., 2003). The volume of LGN extracted from WFU atlas also shows that the left LGN is larger than the right LGN, which means our result is more reliable.

We also investigated sex/age effects on LGN. Our analyses show (i) sex has no effects on LGN volumes; (ii) the LGN volume decreases with increasing age (LGN volumes negatively correlated with human age, shown in Fig. 7). These results are consistent with the previous work (Li et al., 2012). Moreover, plenty of animal experiments have also proved the LGN function will degenerate during the normal aging process (Diaz et al., 1999; de la Roza et al., 1986; Vidal et al., 2004). The LGN shrinkage long with normal aging is consistent with these animal studies (Diaz et al., 1999; de la Roza et al., 1986; Vidal et al., 2004).

In summary, comparing our results with prior work confirms that our automatic LGN segmentation method is reliable to measure LGN volumes.

4.3.2. Glaucoma effects on LGN volumes

In order to further validate the applicability to disease research, we applied our LGN segmentation method to segment LGNs of normal controls and glaucoma patients, and compared the LGN volumes between two groups to investigate glaucoma effects on LGN. Gupta reported glaucoma was associated with both optic nerve degeneration and the LGN and visual cortex in 2006 (Gupta et al., 2006). Our result that volume atrophy exists in bilateral LGN volumes and the mean volume of bilateral LGNs in glaucoma patients is consistent with this study (Gupta et al., 2006).

Moreover, we found that the left LGN volume was negatively correlated with bilateral CDR as well as the right LGN volume was positively correlated with right VF size and had a tendency to positively correlate with left VF size (Fig. 9). VF and CDR are important in glaucoma clinical diagnosis. The smaller the VF, the severer is glaucoma and the greater is the CDR. The negative correlation between the bilateral CDR and the left LGN volume as well as the positive correlation between the bilateral VF size and the right LGN volume is consistent with our expectations that they are related with each other in glaucoma, thus demonstrating that our automatic LGN segmentation method can be applied to disease investigation.

4.4. Comparison with semi-automatic segmentation

The current work is developed based on the semi-automatic segmentation proposed in Li's study (Li et al., 2012). The differences between our work and the semi-automatic method are the prior mask generation, the initial seed chosen and the radius of region growing. Li's study only used the VDC area as the prior mask while our work further restricted the prior mask by intersecting the VDC area with a 7 mm-cube-mask. The initial seed in chosen by experts in Li's study, which lead to the subjectivity and time-consuming of the semi-automatic method. If the initial seed deviates from the real LGN center, a part of LGN will be definitely not be detected in their method. We chosen the initial seed based on the peak active location of LGN, which was obtained by the function imaging study of LGN (Kastner et al., 2004). Our method is objective and is 16–20 times faster than the semi-automatic method. 3 mm in the native space was used as the radius of region growing in Li's study whereas 5 mm in the MNI space was used in our study. Because the normalization processing from the native space to the MNI space enlarges the structures in the brain, the radius of region growing in the MNI

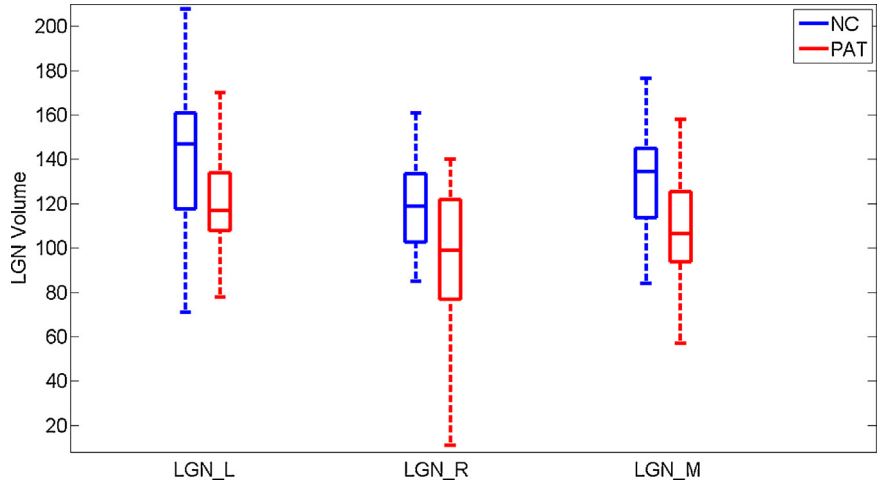

Fig. 8. Glaucoma effects on LGN volume (mm^3). LGN_L: left LGN, LGN_R: right LGN, LGN_M: the mean volume of bilateral LGN, NC: normal controls, PAT: glaucoma patients. Blue represents the LGN volume of normal controls. Red represents the LGN volume of glaucoma patients. (For interpretation of the references to color in this figure legend, the reader is referred to the web version of this article.)

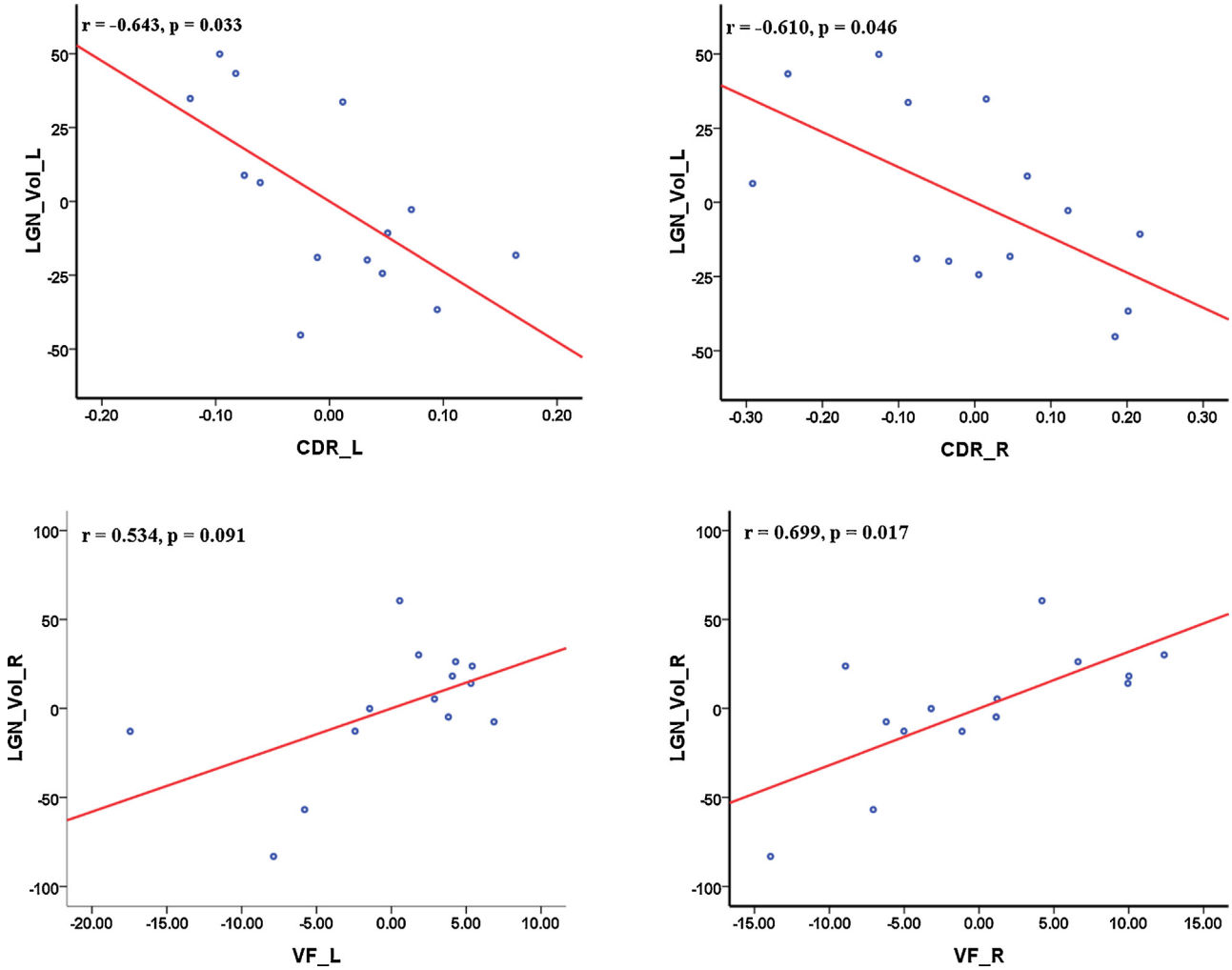

Fig. 9. The relationship between the LGN and clinical parameters in glaucoma patients with age, gender and ICV as control variables. Partial correlation removes the effects of control variables. The axes represent the standardized residuals of corresponding variables removing the effects of control variables. LGN_vol_L/R: left/right LGN volume, CDR_L/R: left/right cup to disk ratio, VF_L/R: left/right visual field.

space is bigger than that in the native space. Considering the error caused by normalization processing, we think the radius in the two method have little influence on the segmented results.

When investigating the LGN volumes of normal controls, our method and Li's method both found that the LGN shrinks with age and the sex has no effects on LGN volumes. But our LGN volume range was a little wider than Li' study and the LGN asymmetry found by us is contrary to Li's result. The main reason of the former difference is that the sample size of our LGN study (280) is much larger than that of Li's study (55), since the individual LGN volume vary about two or three times (Andrews et al., 1997). Although the LGN asymmetry of our work is contrary to that of Li's study, our result is consistent with the asymmetry of LGN extracted from WFU atlas (Maldjian et al., 2003). This demonstrates that our result is more reliable.

4.5. Future work

If some disease has shifted the brain tissue, for example because of a tumor, this would move the LGN outside of the prior-mask-restricted region, and our proposed method would not be able to locate a valid LGN location. However, our method can be applied in the research of clinical vision-related diseases, such as amblyopia, glaucoma and myopia. We also plan to take the LGN shape into consideration in the segmentation and modify our segmented LGN accordingly to address the aforementioned problem. This work is ongoing.

5. Conclusion

In the current study, we presented an objective, efficient, valid, and applicable method of automatic LGN segmentation in vivo. Besides comparing automatically segmented LGN with the manually segmented LGN, we also evaluated the segmented method indirectly by validating the anatomical location of segmented LGN as well as applicability in LGN volumes in normal controls and glaucoma effects on LGN. Our automatic LGN segmentation method will speed up the research on visual system and greatly enhance studies of different vision-related diseases in the future, making MRI-based LGN morphometry in vivo not only faster, but also more objective and reliable.

Acknowledgements

This work was supported in part by 863 Projects (2013AA013803), Youth Innovation Promotion Association CAS, National Natural Science Foundation of China (61271151, 61228103), and ERA-net neuron project "Restoration of Vision after Stroke (REVIS)" and BMBF (grant nr: 01EW1210).

Appendix A. Supplementary data

Supplementary data associated with this article can be found, in the online version, at http://dx.doi.org/10.1016/j.jneumeth.2015.08.006.

References

Adams R, Bischof L. Seeded Region Growing. IEEE Trans Pattern Anal Mach Intell 1994;16:641–7.
Andrews TJ, Halpern SD, Purves D. Correlated size variations in human visual cortex, lateral geniculate nucleus, and optic tract. J Neurosci 1997;17:2859–68.
Ashburner J, Neelin P, Collins DL, Evans A, Friston K. Incorporating prior knowledge into image registration. Neuroimage 1997;6:344–52.
Ashburner J, Hutton C, Frackowiak R, Johnsrude I, Price C, Friston K. Identifying global anatomical differences: Deformation-based morphometry. Hum Brain Mapp 1998;6:348–57.
Barnes GR, Li X, Thompson B, Singh KD, Dumoulin SO, Hess RF. Decreased gray matter concentration in the lateral geniculate nuclei in human amblyopes. Invest Ophthalmol Vis Sci 2010;51:1432–8.
Behrens TEJ, Woolrich MW, Jenkinson M, Johansen-Berg H, Nunes RG, Clare S, et al. Characterization and propagation of uncertainty in diffusion-weighted MR imaging. Magn Reson Med 2003;50:1077–88.
Behzadi Y, Liu TT. An arteriolar compliance model of the cerebral blood flow response to neural stimulus. Neuroimage 2005;25:1100–11.
Chen W, Kato T, Zhu XH, Strupp J, Ogawa S, Ugurbil K. Mapping of lateral geniculate nucleus activation during visual stimulation in human brain using fMRI. Magn Reson Med 1998;39:89–96.
Chen W, Zhu XH, Thulborn KR, Ugurbil K. Retinotopic mapping of lateral geniculate nucleus in humans using functional magnetic resonance imaging. Proc Natl Acad Sci U S A 1999;96:2430–4.
Chen Z, Wang J, Lin F, Dai H, Mu K, Zhang H. Correlation between lateral geniculate nucleus atrophy and damage to the optic disc in glaucoma. J Neuroradiol 2013;40.
Chica MG, Schneider KA. Hemispheric differences in the human lateral geniculate nucleus. J Vis 2013;13:24.
Ciccarelli O, Toosy AT, Parker GJM, Wheeler-Kingshott CAM, Barker GJ, Miller DH, et al. Diffusion tractography based group mapping of major white-matter pathways in the human brain. Neuroimage 2003;19:1545–55.
Dai H, Mu KT, Qi JP, Wang CY, Zhu WZ, Xia LM, et al. Assessment of lateral geniculate nucleus atrophy with 3 T MR imaging and correlation with clinical stage of glaucoma. AJNR Am J Neuroradiol 2011;32:1347–53.
de la Roza C, Cano J, Satorre J, Reinoso-suarez F. A morphologic analysis of neurons and neuropil in the dorsal lateral geniculate nucleus of aged rats. Mech Ageing Dev 1986;34:233–48.
Decourten C, Garey LJ. Morphology of the neurons in the human lateral geniculate-nucleus and their normal development – a golgi-study. Exp Brain Res 1982;47:159–71.
Desikan RS, Segonne F, Fischl B, Quinn BT, Dickerson BC, Blacker D, et al. An automated labeling system for subdividing the human cerebral cortex on MRI scans into gyral based regions of interest. Neuroimage 2006;31:968–80.
D'Esposito M, Deouell LY, Gazzaley A. Alterations in the BOLD fMRI signal with ageing and disease: a challenge for neuroimaging. Nat Rev Neurosci 2003;4:863–72.
Devlin JT, Sillery EL, Hall DA, Hobden P, Behrens TE, Nunes RG, et al. Reliable identification of the auditory thalamus using multi-modal structural analyses. Neuroimage 2006;30:1112–20.
Diaz F, Villena A, Gonzalez P, Requena V, Rius F, Perez De Vargas I. Stereological age-related changes in neurons of the rat dorsal lateral geniculate nucleus. Anat Rec 1999;255:396–400.
Fischl B, Salat DH, Busa E, Albert M, Dieterich M, Haselgrove C, et al. Whole brain segmentation: automated labeling of neuroanatomical structures in the human brain. Neuron 2002;33:341–55.
Fujita N, Tanaka H, Takanashi M, Hirabuki N, Abe K, Yoshimura H, et al. Lateral geniculate nucleus: anatomic and functional identification by use of MR imaging. Am J Neuroradiol 2001;22:1719–26.
Giraldo M, Hegarty JP, Schneider KA. Reduction of the lateral geniculate nucleus volume in subjects with dyslexia compared to matched controls. J Vis 2012;12:536.
Gupta N, Ang LC, de Tilly LN, Bidaisee L, Yucel YH. Human glaucoma and neural degeneration in intracranial optic nerve, lateral geniculate nucleus, and visual cortex. Br J Ophthalmol 2006;90:674–8.
Gupta N, Greenberg G, de Tilly LN, Gray B, Polemidiotis M, Yucel YH. Atrophy of the lateral geniculate nucleus in human glaucoma detected by magnetic resonance imaging. Br J Ophthalmol 2009;93:56–60.
Horton JC, Landau K, Maeder P, Hoyt WF. Magnetic-resonance-imaging of the human lateral geniculate-body. Arch Neurol 1990;47:1201–6.
Hripcsak G, Heitjan DF. Measuring agreement in medical informatics reliability studies. J Biomed Inform 2002;35:99–110.
Kanowski M, Voges J, Tempelmann C. Delineation of the nucleus centre median by proton density weighted magnetic resonance imaging at 3 T. Neurosurgery 2010;66:E-3, discussion E123.
Kastner S, O'Connor DH, Fukui MM, Fehd HM, Herwig U, Pinsk MA. Functional imaging of the human lateral geniculate nucleus and pulvinar. J Neurophysiol 2004;91:438–48.
Korsholm K, Madsen KH, Frederiksen JL, Skimminge A, Lund TE. Recovery from optic neuritis: an ROI-based analysis of LGN and visual cortical areas. Brain 2007;130:1244–53.
Kupfer C, Chumbley L, Downer JC. Quantitative histology of optic nerve, optic tract and lateral geniculate nucleus of man. J Anat 1967;101:393–401.
Lancaster JL, Woldorff MG, Parsons LM, Liotti M, Freitas CS, Rainey L, et al. Automated Talairach atlas labels for functional brain mapping. Hum Brain Mapp 2000;10:120–31.
Li M, He HG, Shi W, Li J, Lv B, Wang CH, et al. Quantification of the human lateral geniculate nucleus in vivo using MR imaging based on morphometry: volume loss with age. AJNR Am J Neuroradiol 2012;33:915–21.
Lu K, Perthen JE, Duncan RO, Zangwill LM, Liu TT. Noninvasive measurement of the cerebral blood flow response in human lateral geniculate nucleus with arterial spin labeling fMRI. Hum Brain Mapp 2008;29:1207–14.
Maldjian JA, Laurienti PJ, Kraft RA, Burdette JH. An automated method for neuroanatomic and cytoarchitectonic atlas-based interrogation of fMRI data sets. Neuroimage 2003;19:1233–9.
McKetton L, Schneider KA. Discriminating the eye-specific layers of the human lateral geniculate nucleus using high-resolution fMRI. J Vis 2012;12:212.

McKetton L, Viviano J, Schneider K. Resolving the individual layers of the human lateral geniculate nucleus using high-resolution structural MRI. J Vis 2013;13:554.
Miki A, Liu GT, Goldsmith ZG, Liu CS, Haselgrove JC. Decreased activation of the lateral geniculate nucleus in a patient with anisometropic amblyopia demonstrated by functional magnetic resonance imaging. Ophthalmologica 2003;217:365–9.
Miki A, Liu CS, Liu GT. Effects of voxel size on detection of lateral geniculate nucleus activation in functional magnetic resonance imaging. Jpn J Ophthalmol 2004;48:558–64.
Putnam TJ. Studies on the central visual system IV the details of the organization of the geniculostriate system in man. Arch Neurol Psychiatry 1926;16:683–707.
Schneider KA, Richter MC, Kastner S. Retinotopic organization and functional subdivisions of the human lateral geniculate nucleus: a high-resolution functional magnetic resonance imaging study. J Neurosci 2004;24:8975–85.
Sherman SM, Koch C. The control of retinogeniculate transmission in the mammalian lateral geniculate nucleus. Exp Brain Res 1986;63:1–20.
Sled JG, Zijdenbos AP, Evans AC. A nonparametric method for automatic correction of intensity nonuniformity in MRI data. IEEE Trans Med Imaging 1998;17:87–97.
Vidal L, Ruiz C, Villena A, Diaz F, Perez de Vargas I. Quantitative age-related changes in dorsal lateral geniculate nucleus relay neurons of the rat. Neurosci Res 2004;48:387–96.
Viviano J, DeSimone K, Schneider K. Intrinsic functional connectivity of the humans lateral geniculate nucleus. J Vis 2012;12:382.
von Noorden GK, Crawford ML. The lateral geniculate nucleus in human strabismic amblyopia. Invest Ophthalmol Vis Sci 1992;33:2729–32.
von Noorden GK, Crawford ML, Levacy RA. The lateral geniculate nucleus in human anisometropic amblyopia. Invest Ophthalmol Vis Sci 1983;24:788–90.
Warfield SK, Zou KH, Wells WM. Simultaneous truth and performance level estimation (STAPLE): an algorithm for the validation of image segmentation. IEEE Trans Med Imaging 2004;23:903–21.
Weber AJ, Chen H, Hubbard WC, Kaufman PL. Experimental glaucoma and cell size, density, and number in the primate lateral geniculate nucleus. Invest Ophthalmol Vis Sci 2000;41:1370–9.
Williams GW. Comparing the joint agreement of several raters with another rater. Biometrics 1976:619–27.
Zhang D, Snyder AZ, Shimony JS, Fox MD, Raichle ME. Noninvasive functional and structural connectivity mapping of the human thalamocortical system. Cereb Cortex 2010;20:1187–94.
Zvorykin VP. New data on individual quantitative features of the human lateral geniculate body. Arkh Anat Gistol Embriol 1980;78:24–7.